ADVANCED MATERIALS
www.advmat.de

Primary Human Breast Cancer-Associated Endothelial Cells Favor Interactions with Nanomedicines

*Lin Wang, Vinit Sheth, Kaili Liu, Prasanta Panja, Alex N. Frickenstein, Yuxin He, Wen Yang, Abigail G. Thomas, Mohammad Hasan Jamei, Jeesoo Park, Shanxin Lyu, Nathan D. Donahue, Wei R. Chen, Resham Bhattacharya, Priyabrata Mukherjee, and Stefan Wilhelm**

Cancer nanomedicines predominately rely on transport processes controlled by tumor-associated endothelial cells to deliver therapeutic and diagnostic payloads into solid tumors. While the dominant role of this class of endothelial cells for nanoparticle transport and tumor delivery is established in animal models, the translational potential in human cells needs exploration. Using primary human breast cancer as a model, the differential interactions of normal and tumor-associated endothelial cells with clinically relevant nanomedicine formulations are explored and quantified. Primary human breast cancer-associated endothelial cells exhibit up to ≈2 times higher nanoparticle uptake than normal human mammary microvascular endothelial cells. Super-resolution imaging studies reveal a significantly higher intracellular vesicle number for tumor-associated endothelial cells, indicating a substantial increase in cellular transport activities. RNA sequencing and gene expression analysis indicate the upregulation of transport-related genes, especially motor protein genes, in tumor-associated endothelial cells. Collectively, the results demonstrate that primary human breast cancer-associated endothelial cells exhibit enhanced interactions with nanomedicines, suggesting a potentially significant role for these cells in nanoparticle tumor delivery in human patients. Engineering nanoparticles that leverage the translational potential of tumor-associated endothelial cell-mediated transport into human solid tumors may lead to the development of safer and more effective clinical cancer nanomedicines.

1. Introduction

The lack of efficient and controlled delivery of intravenously administered nanomedicines to targeted organs, tissues, and cells in the body represents a major challenge in bionanotechnology and is hampering clinical translation.[1] For example, the analysis of preclinical studies published between 2005 and 2015 demonstrated that only ≈1% of the intravenously administrated nanoparticles are delivered to solid tumors.[2] This finding was corroborated in more recent publications.[3] The low nanoparticle delivery efficiency is a consequence of the multitude of biological barriers that compete with the tumor tissue for nanoparticles.[4]

To describe these barriers comprehensively, we recently introduced the term "nanoparticle blood removal pathways" (NBRP) to better define the body's various cell-dependent and cell-independent blood clearance mechanisms.[1] Understanding the interactions between administered nanoparticles and biological systems, including the NBRP, is essential to improving

L. Wang, V. Sheth, K. Liu, A. N. Frickenstein, Y. He, W. Yang, A. G. Thomas, M. H. Jamei, J. Park, S. Lyu, N. D. Donahue, W. R. Chen, S. Wilhelm
Stephenson School of Biomedical Engineering
University of Oklahoma
Norman, OK 73019, USA
E-mail: stefan.wilhelm@ou.edu

P. Panja, P. Mukherjee
Department of Pathology
University of Oklahoma Health Sciences Center
Oklahoma City, OK 73104, USA

The ORCID identification number(s) for the author(s) of this article can be found under https://doi.org/10.1002/adma.202403986

R. Bhattacharya
Department of Obstetrics and Gynecology
University of Oklahoma Health Sciences Center
Oklahoma City, OK 73104, USA

R. Bhattacharya, P. Mukherjee, S. Wilhelm
Stephenson Cancer Center
University of Oklahoma Health Sciences Center
Oklahoma City, OK 73104, USA

S. Wilhelm
Institute for Biomedical Engineering
Science and Technology (IBEST)
Norman, OK 73019, USA

DOI: 10.1002/adma.202403986

the nanoparticle delivery process. Enhancing the nanoparticle delivery efficiency will enable the development of safer and more effective next-generation nanomedicines.[5]

In the context of cancer treatment, current nanomedicines provide some benefits to improve the quality of life for patients.[6] For example, these formulations can decrease systemic toxicity and improve the pharmacokinetics of their small-molecule drug payloads. However, nanomedicines often fail to show enhanced therapeutic efficacy, which is attributed partially to the overall low nanoparticle delivery efficiency to solid tumors.[7] To address this shortcoming, there is an urgent need to better understand nanoparticle tumor delivery.

Nanoparticle tumor delivery is a complex multistep process.[8] In this study, we focus on the first step. That is, when nanoparticles reach solid tumor tissues upon circulation in the bloodstream, they first need to overcome the blood vessel walls of the endothelium to reach malignant cells in the tumor microenvironment.[9] The endothelium wall is formed by a layer of so-called endothelial cells. Within the solid tumor tissue, these cells are referred to as tumor-associated endothelial cells.[8c,10]

Discontinuous endothelium in the spleen and some solid tumors, and fenestrated endothelial cells in the liver and kidney facilitate increased nanoparticle transport across the vessel walls.[1,11] However, Sindhwani et al. reported recently that the frequency of endothelial gaps along tumor vasculature is insufficient to account for the observed nanoparticle accumulation in solid tumors. Their study revealed that up to 97% of nanoparticles enter solid tumors by interacting with tumor-associated endothelial cells.[12] Specifically, these cells internalize the nanoparticles and transport them actively across the cell lumen to release the nanoparticles on the opposite side. This transport process is referred to as transcytosis and allows nanoparticles to reach malignant cells within the tumor stroma.[8a,13]

En route to solid tumors, nanoparticles interact with endothelial cells that form the inner wall of blood vessels. Nanoparticles must transport from the luminal to the abluminal side of tumor blood vessels to reach cancer cells, which requires interactions with tumor-associated endothelial cells. We wondered whether these interactions are different for tumor-associated endothelial cells compared to normal endothelial cells. This is an important question because preferential interactions of nanoparticles with tumor-associated endothelial cells could potentially be exploited for increased solid tumor delivery, which may result in safer and more effective nanomedicine-based treatments. In addition, studies have shown that tumor-associated endothelial cells adjust to the tumor microenvironment and exhibit changes in morphological, cytogenetic, epigenetic, gene expression, metabolism, and drug-resistant behavior compared to normal endothelial cells.[10,14] These differences further motivated us to investigate and compare nanoparticle interactions between normal and tumor-associated endothelial cells.

For our study, we selected primary human endothelial cells from breast tissue as model systems with clinical relevance. Primary human mammary microvascular endothelial cells (HMMECs) represent the normal (i.e., healthy breast tissue) control cells to establish the baseline interactions with nanoparticles. We then used primary human tumor-associated endothelial cells (HBTECs) to characterize and quantify the differential nanoparticle interactions. First, we compared the nanoparticle internalization efficiency and internalization pathways for these two endothelial cell types. Next, we studied the differences in nanoparticle cell transport by comparing the endocytosis pathway activity, intracellular transport features, and gene expression levels between these two cell types. Understanding the differential nanoparticle interactions between normal and tumor-associated endothelial cells is essential in furthering our understanding of the nanoparticle tumor delivery process and guiding the design of cancer nanomedicines that are safer and more effective.

2. Results and Discussion

2.1. Tumor-Associated Endothelial Cells Favor Interactions with Administered Nanoparticles

We first compared the uptake efficiency of nanoparticles between tumor-associated and normal endothelial cells (**Figure 1**). We selected three different types of model nanoparticles that represent a broad range of preclinically and clinically used formulations: i) PEGylated gold nanoparticles,[15] ii) liposomal doxorubicin (Doxove),[16] and iii) 3,3′-dioctadecyloxacarbocyanine perchlorate-labeled lipid nanoparticles (DiO-LNPs).[17] Figure S1 and Table S1 (Supporting Information) summarize the physicochemical characterization data of these nanoparticles, as well as the incubation concentrations during cell uptake. We selected gold nanoparticles because they: i) can be quantified precisely within tissues and cells by inductively coupled plasma mass spectrometry, ii) can be synthesized with narrow size distribution and controlled surface chemistry, and iii) are biocompatible and remain stable under cell culture conditions for an extended time period.[18] We also selected liposomal doxorubicin (Doxoves) nanoparticles that represent one of the major nanomedicine-based chemotherapeutics in clinical breast cancer treatment.[19] As the third model nanoparticle, we selected LNPs, as they are widely used in some COVID-19 vaccine formulations and are an emerging class of nanomedicines.[20] Liposomal doxorubicin and LNPs are, therefore, model nanomedicines with high clinical significance.

In our first set of experiments, we used PEGylated gold nanoparticles and incubated them together with different types of primary human endothelial cells from healthy and tumor breast tissues. We selected breast tissue cells as a model system because nanomedicines are used in the clinic for some types of breast cancer treatments.[21] In addition, breast cancers form solid tumor masses with blood vessels that intravenously administered nanoparticles need to overcome for safe and effective delivery. Nanoparticle interactions with vascular endothelial cells are, therefore, a critical first step in the overall delivery process.

We performed three different types of cell culture experiments. The first experiment used general endothelial cell culture media with fetal bovine serum (FBS). The second experiment used conditioned media with FBS (Figure S2, Supporting Information), and the third experiment used general media with human serum. Our rationale for the use of conditioned cell culture media was to mimic better the microenvironmental characteristics of healthy and tumor breast tissue. Therefore, we used conditioned cell culture media containing the media from breast tumor cells, MDA-MB-231, and nontumor breast epithelial cells, MCF-10a, respectively. Using SDS-PAGE, we observed different protein profiles in

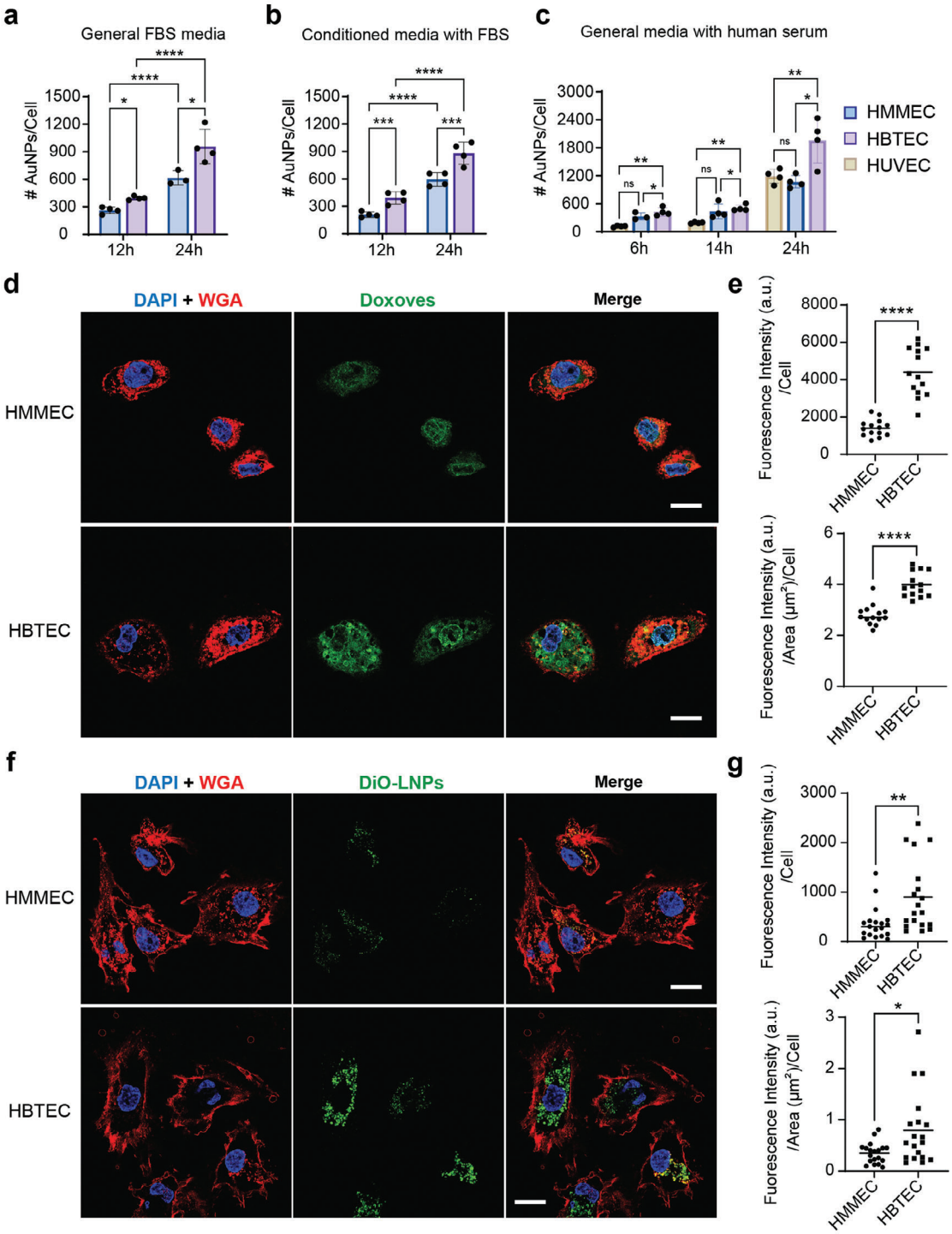

Figure 1. Breast tumor-associated endothelial cells favor interactions with nanoparticles. a–c) Gold nanoparticle uptake comparison between HMMECs and HBTECs under three different cell culture conditions as quantified by inductively coupled plasma mass spectrometry (ICP-MS): a) general cell culture media with FBS, b) conditioned cell culture media (containing media collected from nontumoral breast epithelial cell and breast tumor cell cultures for HMMEC and HBTEC, respectively) with FBS, and c) general cell culture media with human serum. Bar graphs present the mean ± standard deviation ($n = 4$). Statistical tests were performed by two-way ANOVA. AuNPs, gold nanoparticles. d) Liposomal doxorubicin (Doxoves, green) uptake comparison using confocal laser scanning microscopy (CLSM). The cells were stained with DAPI (blue) and WGA-CF633 (red). e) Quantitative image analysis of liposomal doxorubicin uptake by ImageJ. f) Lipid nanoparticle (LNP) uptake comparison using CLSM. LNPs were labeled with DiO (green), while cells were stained with DAPI (blue) and WGA-CF633 (red). g) Quantitative image analysis of LNPs uptake by ImageJ. Image analysis plots present individual values with the line indicating the mean value. Statistical tests for image analysis were performed by unpaired two-tailed *t*-test ($n = 14$ for liposomes, $n = 19$ for LNPs). Scale bar, 20 μm. HMMEC, human mammary microvascular endothelial cell; HBTEC, human breast tumor-associated endothelial cell. $^{*}p \leq 0.05$, $^{**}p \leq 0.01$, $^{***}p \leq 0.001$, $^{****}p \leq 0.0001$, ns indicates a nonsignificant difference.

the cell culture media collected from MDA-MB-231 and MCF-10a cell cultures (Figure S3, Supporting Information), indicating different secretory profiles of the two cell types. For the third cell culture media condition, we replaced the FBS proteins with human serum to evaluate the effect of human proteins on nanoparticle endothelial cell interactions. As an additional control group, we used normal human umbilical vein endothelial cells (HUVECs). HUVECs are often used in the literature to study nanoparticle endothelial cell interactions.[22]

Upon exposure of endothelial cells to gold nanoparticles, we used ICP-MS as a quantitative method to determine nanoparticle–cell interactions. Interestingly, in all three experiments conducted with different media and at different tested incubation time points, tumor-associated HBTECs endothelial cells exhibited a consistently stronger interaction with gold nanoparticles compared to control cells (HMMECs, HUVECs), reaching up to ≈1.9 times, as determined by quantitative ICP-MS measurements (Figure 1a–c). We observed that the nanoparticle interactions did not vary significantly between general and conditioned cell culture media with FBS (Figure S4, Supporting Information). Therefore, we used the general FBS-contained endothelial cell complete media for most of the subsequent experiments.

In addition to inorganic gold nanoparticles, we further assessed the nanoparticle interactions of two different organic nanoparticles with these endothelial cells. We incubated the HBTECs and HMMECs with liposomal doxorubicin (Doxoves) or DiO-LNPs for 24 h, followed by staining of cell membrane glycoproteins with wheat germ agglutinin (WGA)-CF633 and nuclei with 4′,6-diamidino-2-phenylindole (DAPI). Confocal laser scanning microscope (CLSM) images revealed stronger fluorescence signals in HBTECs than HMMECs for both nanoparticle types, indicating higher uptake of these organic nanoparticle formulations in tumor-associated endothelial cells (Figure 1d,f; Figures S5 and S6, Supporting Information).

To evaluate the nanoparticle interactions with the endothelial cells more quantitatively, we performed image analysis using two different metrics: i) fluorescence intensity per cell, and ii) fluorescence intensity per cell area, to eliminate any potential cell size confounders (Figure 1e,g). Our results demonstrate that HBTECs exhibit higher fluorescence intensity than HMMECs endothelial cells.

As demonstrated in the literature, nanoparticle physicochemical properties, such as size, composition, and stiffness, affect cell internalization mechanisms and efficiencies.[1] We want to emphasize that our three model nanoparticles cover a range of different sizes (≈70–90 nm hydrodynamic diameter), compositions, and stiffness (gold nanoparticles vs softer organic nanoparticles). Across these different tested nanomaterials, we observed higher interactions for HBTECs, indicating that tumor-associated endothelial cells generally favor interactions with nanomedicines compared to normal endothelial cells.

2.2. Nanoparticles Enter Tumor-Associated Endothelial Cells through Endocytosis

Next, we wondered how nanoparticles enter endothelial cells and whether tumor-associated and normal endothelial cells use similar uptake pathways. While nanoparticle internalization typically results in the formation of intracellular vesicles to transport cargo across cells, these vesicles often exhibit sizes below the diffraction limit of standard light microscopes.[8a,23] To overcome the diffraction limitation, we applied 3D super-resolution light microscopy through a process known as expansion microscopy (ExM).[24] We used a specific ExM method called Magnify, which allows for up to an ≈11-fold increase in lateral resolution on standard light microscopes.[25]

The HBTECs and HMMECs were incubated with gold nanoparticles for 24 h and then stained with AF488-NHS ester dyes that conjugate to proteins via available amine chemical groups (so-called pan stain). The fluorescence-based pan staining provides the required imaging contrast to visualize intracellular features. Since intracellular vesicles are primarily fluid-filled compartments, these features can be clearly differentiated against the protein-rich, and thus fluorescently labeled, cytoplasm. We imaged the intracellular gold nanoparticles in a label-free manner through scattered light imaging. No nanoparticle fluorophore labeling was needed. This approach is benefical, as changes in nanoparticle surfac chemistry through fluorophore labeling, could potentially affect the nanoparticle cell internalization pathways.[26]

Upon cell expansion, we observed enhanced visibility of intracellular vesicles with nanoparticles distinctly localized inside these vesicular structures (**Figure 2**a and Figures S7 and S8, Supporting Information). This finding indicates that nanoparticles tend to enter endothelial cells via endocytosis. In addition, we observed more pronounced and more frequent light scattering signals in HBTEC compared to HMMEC endothelial cells. These qualitative findings suggest that more nanoparticles were taken up by HBTECs, which is consistent with our previous results that HBTECs favor nanoparticle interactions (Figure 1a).

There are three major endocytic pathways involved with nanoparticle uptake: i) caveolin-mediated endocytosis, ii) clathrin-mediated endocytosis, and iii) macropinocytosis. To identify the specific pathways HBTECs and HMMECs employ, we conducted endocytosis-inhibiting assays and quantified the nanoparticle cellular uptake levels. Two or three small molecule inhibitors targeting different steps in each pathway were selected with N-ethylmaleimide (NEM), filipin, and indomethacin for caveolin-mediated endocytosis, chlorpromazine and chloroquine for clathrin-mediated endocytosis, and 5-(N-ethyl-N-isopropyl) amiloride (EIPA), cytochalasin D, and imipramine for macropinocytosis, respectively (Table S2, Supporting Information).[8a]

We first screened the safe working concentrations of each inhibitor (Figures S9 and S10, Supporting Information; and Table S2, Supporting Information). Given that the cytotoxicity of small molecule inhibitors is dose-dependent, we collected the concentration ranges used in other cell lines from the literature as reference screening ranges and performed a cell viability assay with the addition of inhibitors at different concentrations. The highest concentration not exhibiting statistically significant cytotoxicity was selected as the working concentration to ensure both safety and the best inhibitory effect.

We pretreated the cells with the inhibitors for one hour and then incubated them with gold nanoparticles in the presence of inhibitors for 6 and 12 h. Compared to the control group, these inhibitors exhibited a reduction in nanoparticle cell uptake

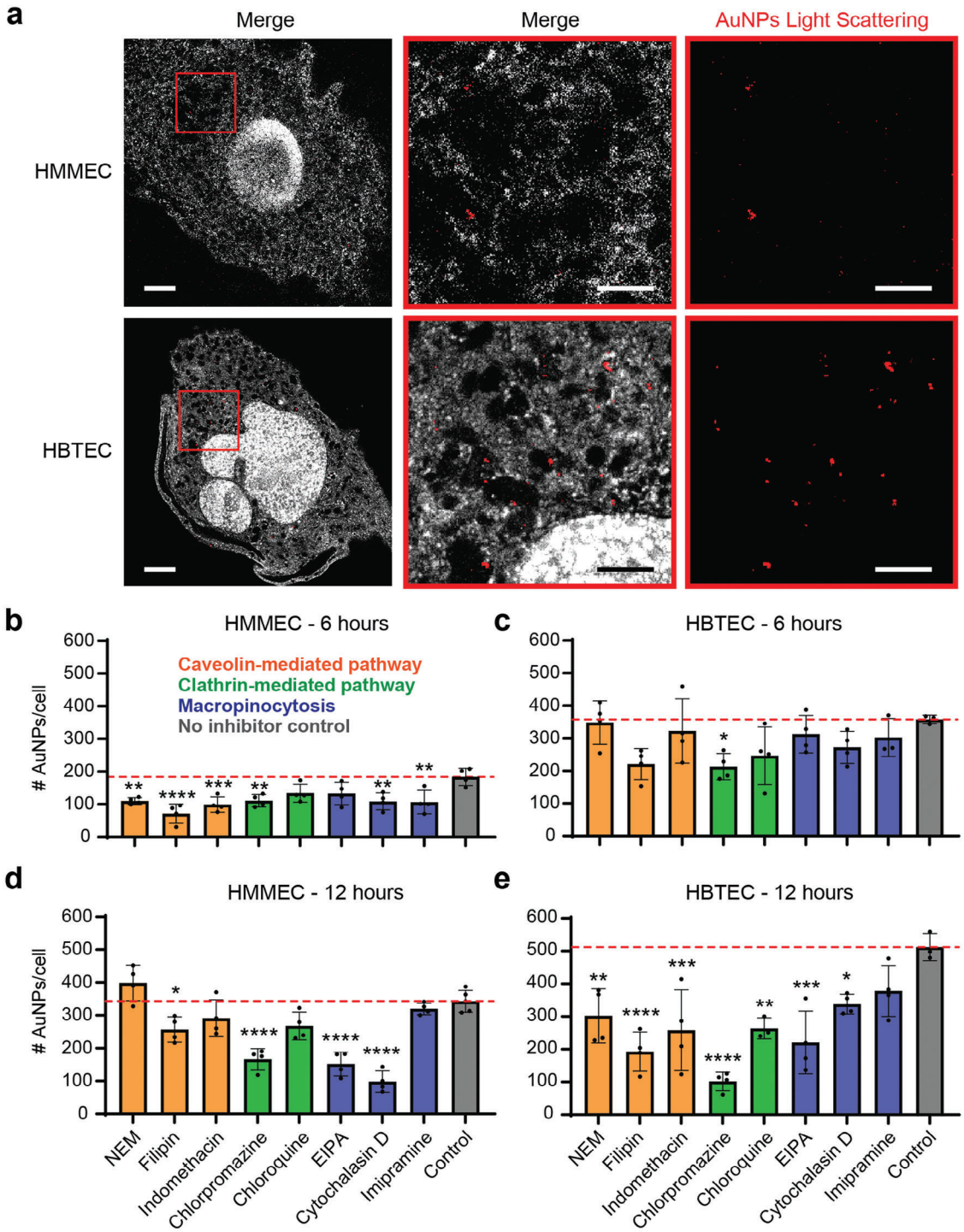

Figure 2. Gold nanoparticles enter endothelial cells through endocytosis and are colocalized in intracellular vesicles. a) Label-free CLSM imaging of gold nanoparticles in expanded HMMECs and HBTECs. After incubation with gold nanoparticles for 24 h, the cells were stained with NHS-AF488 and then expanded using the Magnify protocol for super-resolution imaging. The overlay of stained cells (gray) and gold nanoparticles through light scattering (red) is displayed first, followed by a magnification of all the channels and, finally, the isolated light-scattering channel. Nanoparticles colocalized with the intracellular vesicles. Scale bar in unmagnified images, 25 µm; scale bar in magnified images, 10 µm. b–e) Internalization pathway identification by endocytosis inhibition in HMMECs and HBTECs at different time points. Inhibitors for the three major endocytosis pathways, caveolin-mediated endocytosis, clathrin-mediated endocytosis, and macropinocytosis, were added during nanoparticle incubation. The cellular uptake of nanoparticles in each group was quantified by ICP-MS and compared with the noninhibitor control group. Bar graphs present the mean ± standard deviation (n = 3/4). One-way ANOVA was used for statistical tests. *$p \leq 0.05$, **$p \leq 0.01$, ***$p \leq 0.001$, ****$p \leq 0.0001$. NEM, N-ethylmaleimide; EIPA, 5-(N-ethyl-N-isopropyl) amiloride.

at different levels. However, the inhibiting patterns between HBTECs and HMMECs were similar, as measured by ICP-MS (Figure 2b–e). When testing the caveolin-mediated endocytosis pathway, filipin exhibited higher inhibition efficiency (up to 62.4%) than NEM and indomethacin (up to 41.0% and 49.6%, respectively). Filipin inhibits endocytosis by removing cholesterol, a key component of caveolin-mediated endocytosis, from the plasma membrane. Chlorpromazine (inhibition up to 80.2%) exhibited stronger inhibition than chloroquine (up to 48.5%) when assessing the clathrin-mediated endocytosis pathway. Chlorpromazine functions by translocating clathrin and adaptor protein complex-2, a protein intermediating the binding between clathrin and cell membrane, from the plasma membrane into intracellular vesicles. This action prevents the formation of clathrin-coated pits on the cell membrane for endocytosis. We did not observe a consistent pattern when testing the macropinocytosis inhibition. These results indicate that the three major endocytosis pathways were all involved in gold nanoparticle internalization in both HBTECs and HMMECs.

2.3. Tumor-Associated Endothelial Cells Exhibit Higher Endocytosis Activity

Our previous results showed that tumor-associated endothelial cells interact more strongly with nanoparticles. This finding applies broadly to nanoparticles with different physicochemical properties, such as size, composition, and surface chemistry, as demonstrated in Figure 1. Based on these observations, we hypothesized that the observed preference of tumor-associated endothelial cells to interact with nanoparticles is an inherent property of these cells.

To test this hypothesis, we first compared the endocytosis pathway activity between HBTECs and HMMECs. We used pathway-specific molecular tracers (i.e., albumin for the caveolin-mediated pathway, transferrin for the clathrin-mediated pathway, and 70-kDa Dextran for the macropinocytosis pathway). Literature reports correlate the cell uptake capability of each of the three selected molecular tracers to the relative activity of the corresponding cell uptake pathway.[27] We compared the cellular uptake of the fluorophore-labeled molecular tracers for HBTECs and HMMECs using flow cytometry (**Figure 3**). Our flow cytometry data showed that most HBTEC live cells exhibited overall higher interactions with all three tracers compared to HMMECs. The 70-kDa Dextran tracer exhibited a more substantial difference in cell uptake, being ≈62% higher in HBTECs than in HMMECs, compared to the other two tracers, with an uptake difference of ≈30% for both. These results indicate that tumor-associated endothelial cells exhibit a generally higher endocytosis activity than normal endothelial cells. Next, we studied the expression level of caveolin-1 and clathrin, which are essential proteins in caveolin-mediated and clathrin-mediated pathways, respectively (**Figure 4**). Caveolae are membrane invaginations that are enriched with cholesterol, with caveolin-1, a cholesterol-binding protein, serving to induce membrane curvature toward the formation of vesicles.[28] Clathrin is a trimeric protein that is composed of three heavy chains that are bound at a vertex with light chains. While clathrin does not bind to cell membranes directly, it plays a critical role in the formation of clathrin-coated pits through adapter proteins, which invaginate with the associated cargo, and then scission off to form clathrin-coated vesicles.[29]

Using immunofluorescence staining, we observed higher caveolin-1 and clathrin expression levels in HBTECs than HMMECs (Figure 4a,c) before nanoparticle incubation. After nanoparticle incubation, an increased expression for both proteins was observed in HMMECs at a level similar to that of HBTECs (Figure 4b,d). These results corroborated that tumor-associated endothelial cells exhibit a generally higher activity than normal endothelial cells for both caveolin-mediated and clathrin-mediated endocytosis pathways at a molecular level, which is consistent with our previous endocytosis tracer cell uptake results.

In addition, we could clearly observe the redistribution of caveolin-1 from the middle of the cytoplasm to the near membrane area after nanoparticle incubation (Figure 4c,d). This observation may indicate that caveolin-1 was recruited to the cell membrane for nanoparticle endocytosis and further confirms the involvement of the caveolae-mediated pathway in nanoparticle internalization.

We conducted further investigations into caveolin-1 and clathrin expression levels before and after nanoparticle incubation using western blot analysis (Figure 4e,f). In HMMECs, the expression levels of both proteins increased following nanoparticle incubation, while in HBTECs, the expression levels remained similar. These findings align with the immunostaining results. The above endocytosis tracer uptake and protein expression results support the conclusion that tumor endothelial cells generally exhibit more active endocytic processes than the cells from healthy mammary tissue.

2.4. Tumor-Associated Endothelial Cells Possess Higher Intracellular Vesicle Number

We then investigated the difference in intracellular transport features between the two types of endothelial cells. We imaged HBTECs and HMMECs by super-resolution ExM, as shown in Figure 2a. The images show the intracellular vesicles within the cytoplasm due to the contrast difference between the vesicular area and the cytoplasm after pan protein staining (**Figure 5**a,b).

In representative cells, HBTEC exhibited a higher vesicle number than HMMEC on a per-cell basis (Figure 5a,b; Videos S1 and S2, Supporting Information). Comparing the cell membrane area, the HMMEC cell surface appeared smooth (Figure 5a,i), whereas the HBTEC membrane was densely aligned with vesicle-like structures (Figure 5b,i), indicating the possibility of endocytosis events, potentially accompanied by exocytic processes. The distributions of the intracellular vesicles in the cytoplasm appear to be different as well. Vesicles were primarily located around the nucleus in HMMEC (Figure 5a,ii), whereas dispersed over almost the entire cytoplasm from membrane to nucleus in HBTEC (Figure 5b,ii) endothelial cells. The dense distribution of intracellular vesicles observed in HBTECs may increase the possibility of connecting vesicles that could potentially favor the formation of vesicle channels or vesiculo-vacuolar organelles (VVOs). The presence of such VVOs could potentially further increase the efficiency of intracellular nanoparticle transport and extravasation. The heightened presence of transport vesicles and VVOs

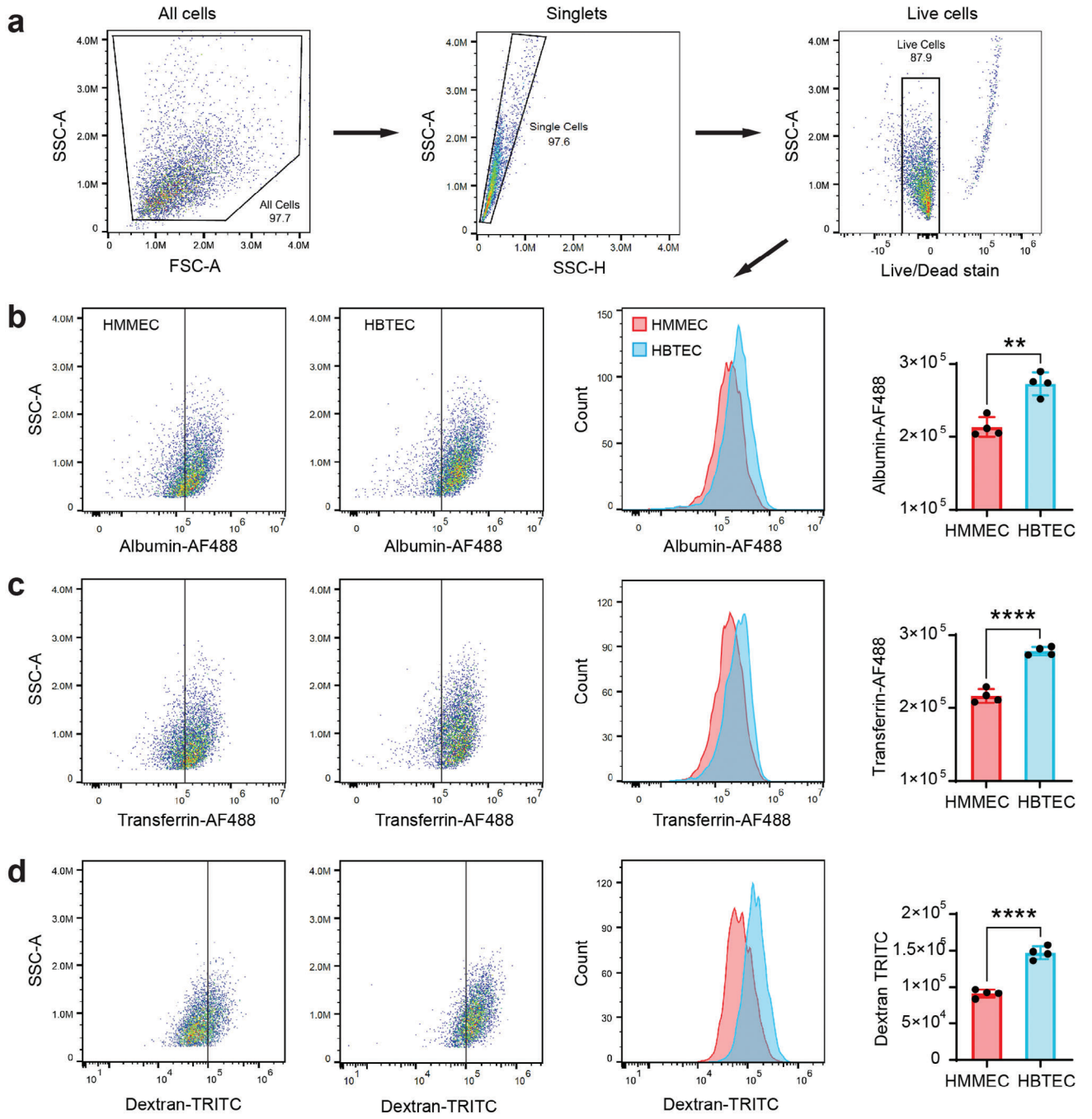

Figure 3. Tumor-associated endothelial cells exhibit higher endocytosis activity than normal endothelial cells. Albumin, transferrin, and dextran (70 kDa), which are pathway tracers of the caveolin-mediated pathway, clathrin-mediated pathway, and macropinocytosis, respectively, were first added to cell media and incubated for one hour. The amount of endocytic tracers was compared between two types of endothelial cells by flow cytometry. a) Gating strategy. b–e) Uptake comparison of albumin-AF488, transferrin-AF488, and Dextran-TRITC. Left two, representative flow cytometry plots of live HMMECs and HBTECs that interacted with fluorescence-labeled tracers. A vertical line was added to facilitate the visualization of cell population position change. The following histograms present the comparison of HMMEC and HBTEC in one plot. Finally, the bar graphs present the mean ± standard deviation of replicate samples ($n = 4$). Unpaired t-tests were performed for statistical analysis. $^{**}p \leq 0.01$, $^{****}p \leq 0.0001$.

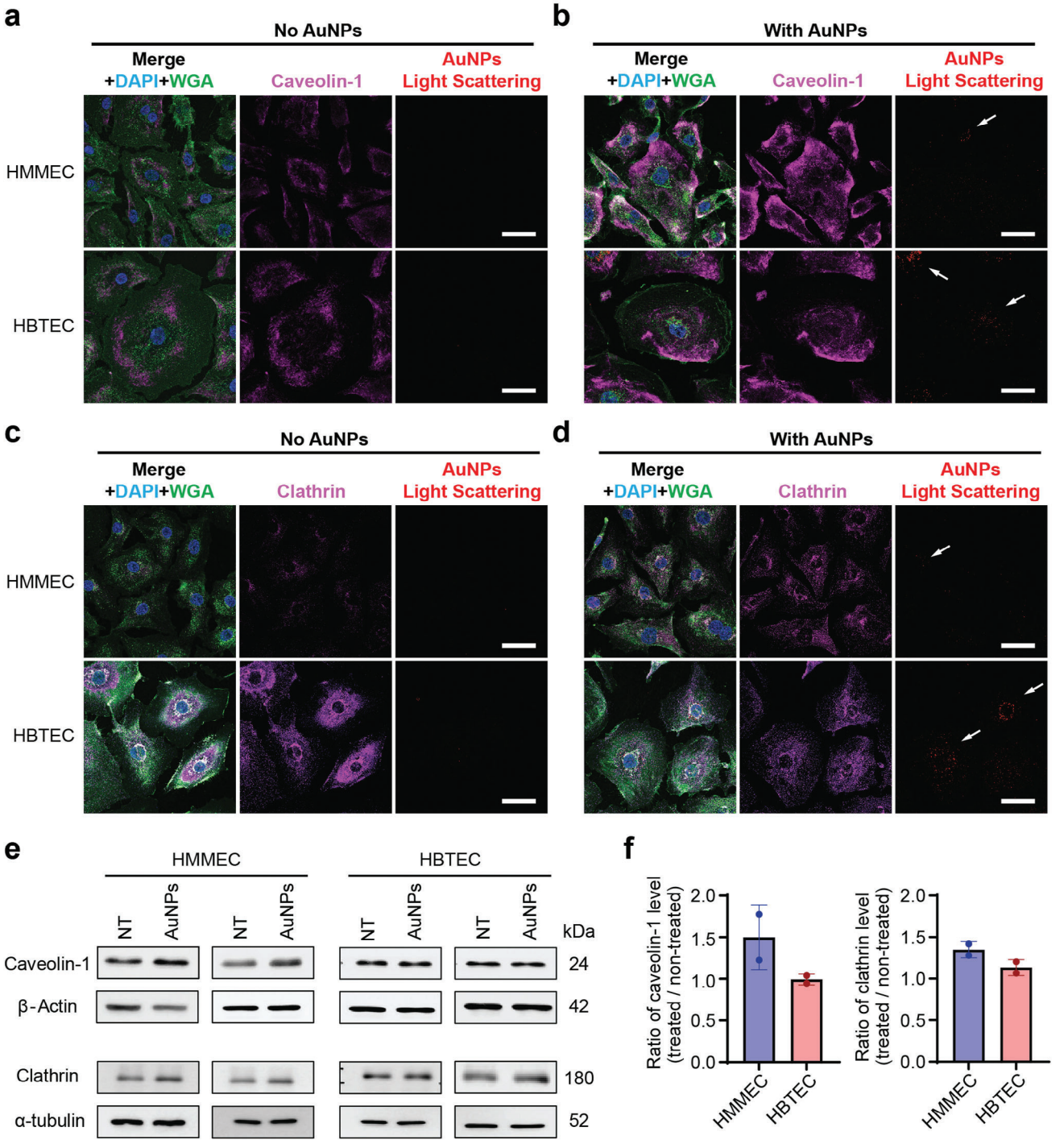

Figure 4. Expression of endocytosis-associated proteins in tumor-associated and normal endothelial cells before and after nanoparticle incubation. a–d) Immunostaining was performed on caveolin-1 and clathrin heavy chain (magenta), which are essential proteins in caveolin-mediated and clathrin-mediated pathways, respectively. Cells were then stained with DAPI (blue) and WGA-CF633 (red). Gold nanoparticles (AuNPs) were detected by light scattering imaging (red). a) Caveolin-1 staining in cells without nanoparticle incubation. b) Caveolin-1 staining in cells after 24-h nanoparticle incubation. c) Clathrin heavy chain staining in cells without nanoparticle incubation. d) Clathrin heavy chain staining in cells after 24-h nanoparticle incubation. The scale bar in all images represents 50 μm. The white arrows indicate the positions of gold nanoparticles. e) Comparison of caveolin-1 and clathrin expression levels before and after nanoparticle incubation by western blot. NT is non-treated; AuNPs groups are treated with gold nanoparticles. f) Densitometry analysis of protein level change after nanoparticle treatment in panel (e). The bars present the mean ± standard deviation of replicate comparisons ($n = 2$).

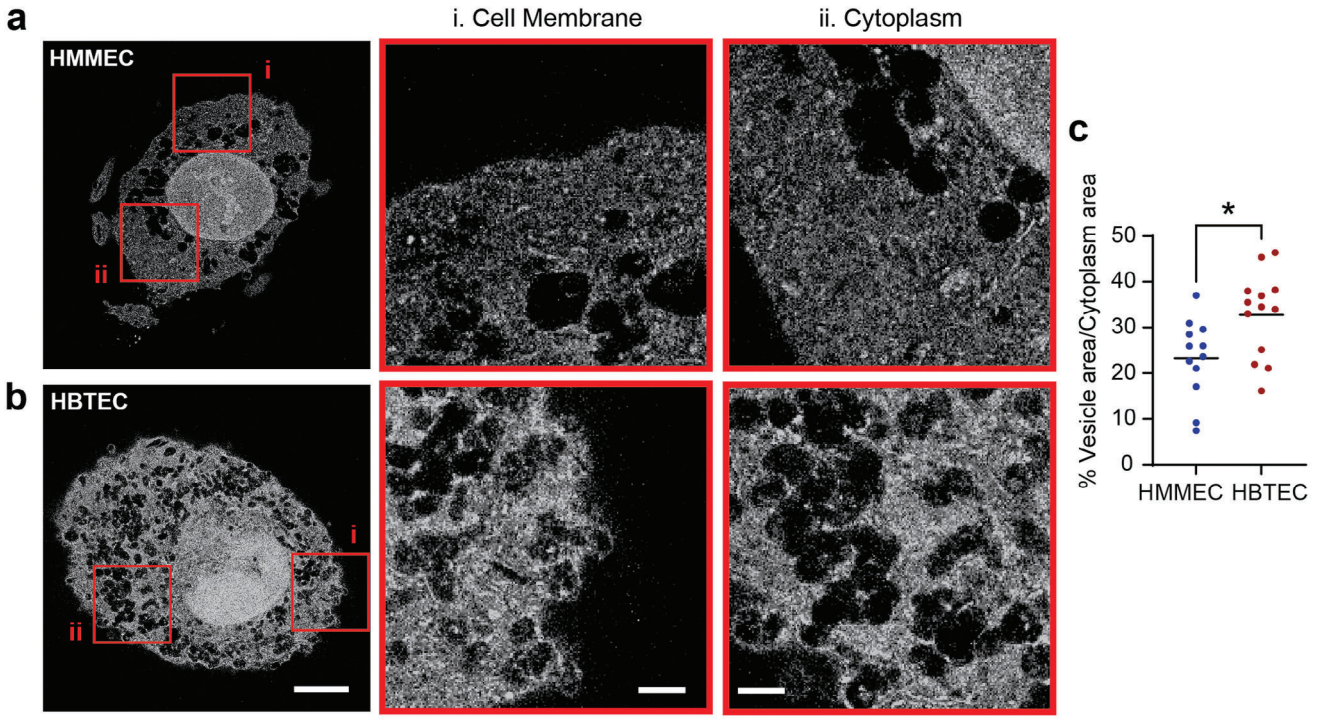

Figure 5. Visualization and comparison of intracellular transport structures through expansion microscopy-based super-resolution imaging. (Left) Representative cells of a) HMMEC and b) HBTEC after the expansion process. The intracellular vesicles are clearly visible as black areas within the cytoplasm. The HBTEC group presents a higher vesicle frequency than the HMMEC group. (Middle) The magnified images of the cell membrane area. (Right) The magnified images of the cytoplasm. Scale bars apply to both (a) and (b). Scale bar in unmagnified images (left), 50 µm; scale bar in magnified images (middle and right), 10 µm. c) Quantitative image analysis was used to compare the intracellular vesicle area. We used ImageJ to analyze the percentage of total vesicle area within the cytoplasm area of each cell. The plot presents individual values with the line indicating the mean value. Statistical tests for image analysis were performed by unpaired two-tailed *t*-test ($n = 12–13$). *$p \leq 0.05$.

was similarly noted in hepatocellular carcinoma endothelial cells using transmission electron microscopy in a prior study.[30]

We observed that the vesicle frequencies between different cells for the same cell type were not uniform. This may be explained by the heterogeneity of cells within the vascular endothelium.[9,30] The plot in Figure 5c represents our quantitative image analysis results. The data suggest that tumor-associated endothelial cells overall exhibit a higher mean of vesicle area/cytoplasm ratio (≈32.8%) than normal endothelial cells (≈23.3%), although some overlap was observed in the two populations.

Overall, this observed higher frequency of intracellular vesicles further supports our finding that tumor-associated endothelial cells perform more active vesicle/vacuole-dependent transport than normal endothelial cells. Together with the previous results of higher endocytic pathway activity and expression of essential protein for endocytosis, the increased uptake of nanoparticles in tumor-associated endothelial cells may be due to their generally higher endocytosis and intracellular transport activities when compared to normal endothelial cells. This hypothesis aligns with the special pathophysiological properties of tumor blood vessels. Cancer cells possess accelerated proliferation, growth, and division compared to normal cells. To support the cancer cell's enhanced proliferation, more mass (e.g., nutritional molecules, oxygen, and water) needs to be transported through the endothelial layer, from the vessel lumen to the abluminal tumor side.[31] Previous studies have identified upregulation of nutrient transporters for glucose, lactate and amino acids in tumor endothelial cells, along with the presence of transendothelial cell "pores" and functional VVO structures facilitating macromolecule transport.[32] These phenotypic changes may relate to an abnormal microenvironment. Understanding the correlation and interplay between increased nanoparticle uptake, tumor vessel behavior, and the tumor microenvironment requires further investigation in future research.

2.5. Gene Expression Profiles Suggest Higher Intracellular Transport in Tumor-Associated Endothelial Cells

Next, we then systematically investigated the difference between the two types of endothelial cells at a molecular level through RNA sequencing (Table S3, Supporting Information). Four groups, HBTECs and HMMECs, with and without gold nanoparticle incubation, were compared in a pairwise manner. The differentially expressed genes in each comparison are summarized in Table S4 and Figure S12 (Supporting Information). Genes with an adjusted *p*-value <0.05 and an absolute log2-fold change > 1 were defined as differentially expressed genes (DEGs). Using this approach, we identified 3953 and 2123 DEGs in the comparisons between HBTEC and HMMEC, under the condition without and with nanoparticle treatment

(HBTEC versus HMMEC, and HBTEC-Au versus HMMEC-Au), respectively. However, only 2 and 25 DEGs were identified for HBTECs and HMMECs, respectively, in the comparison between groups without and with nanoparticle incubation (HBTEC-Au vs HBTEC, and HMMEC-Au vs HMMEC). These results suggest that the gene expression difference is mainly between the two types of endothelial cells, but the treatment by gold nanoparticles did not induce much transcriptome change.

We focused on the analysis of our sequencing results between HBTECs and HMMECs with nanoparticle treatment (**Figure 6**). Among 2123 DEGs, 752 were upregulated, and 1371 were downregulated in HBTECs compared to HMMECs (Figure 6a). We identified multiple genes related to transport in upregulated DEGs by studying the ones with the lowest adjusted p-value and highest log2-fold change. Gene *LRP5* encodes a transmembrane low-density lipoprotein receptor and was upregulated to 3.5 times in HBTECs. The encoded receptor binds and internalizes ligands through clathrin-mediated endocytosis. *KIF19* and *MYO7A* encode proteins in kinesin and myosin motor protein families and were increased to 4.3- and 8.7-folds, respectively. *SELP*, with a 7.7-fold upregulation, encodes the protein selectin P, which is a membrane receptor binding to carbohydrates and derivatives, and related to nanoparticle uptake through caveolae-mediated endocytosis.[13a,33] *EXOC3L2*, upregulated to 19.9-folds, encodes a protein in an exocyst complex that functions in tethering secretory vesicles to the plasma membrane. The protein can be upregulated by vascular endothelial growth factor A. No specific genes from the downregulated DEGs were identified using the same strategy.

We performed gene ontology (GO) enrichment analyses using the upregulated DEGs in two different databases, David and Toppgene (Figure 6b and Figure S13, Supporting Information). The two analyses gave similar results, i.e. that GO categories related to transport were enriched. Figure 6b shows that positive regulation of intracellular transport, ATP-dependent microtubule motor activity, and kinesin complex were enriched by 14.9-, 11.6-, and 8.7-folds, respectively. Kinesins are motor proteins that transport different cargos including vesicles along the microtubule system to the appropriate destination.[34] A GO category, actomyosin structure organization, linked to another type of motor protein, myosin, was also enriched (Figure 6b). Myosins can transport vesicles along actin filaments for relatively short-range distribution.[35] These instances demonstrate that tumor-associated endothelial cells exhibit increased expression of genes related to transportation, with a particular emphasis on motor protein genes.

We then studied the gene expression profile in kinesin, dynein, and myosin families (Figure 6c). Kinesins and dyneins are both microtubule-based motor proteins, with kinesins moving toward microtubule plus ends (from cell interior toward periphery) while dyneins toward minus ends (from cell periphery to cell interior).[36] We found that ≈63% and ≈52% of the sequenced genes were statistically significantly changed in the kinesin and myosin families, respectively, while only ≈30% changed in the dynein family. In addition, heatmaps, presented in Figure 6c, showing the expression of each gene, demonstrate that there are more genes upregulated than downregulated in the kinesin and myosin families, which contrasts with the overall cell expression pattern. These findings provide additional evidence supporting the enhanced prevalence and possibly activity of motor proteins (especially kinesins and myosins) in tumor-associated endothelial cells. The elevated expression of kinesin and myosin proteins was observed in human ovarian carcinoma-associated endothelial cells as well in a previous analysis of gene expression profiles.[37]

Inspired by the motor protein analysis, we further studied the gene expression profile in each category in the membrane trafficking process (Figure 6d and Figures S14–S17, Supporting Information). Membrane trafficking describes the intricate process through which proteins and other macromolecules are internalized, distributed within the cell, and released outside the cell using membrane-bound vesicles. The percentage plot (Figure S14, Supporting Information) shows that 38.0%, 29.5%, 23.0%, 34.8%, 21.1%, and 40.6% of the sequenced genes were statistically significantly changed in endocytosis, endosome-Golgi transport, endosome-lysosome transport, exocytosis, SNARE, and other categories, respectively, indicating an essential difference in membrane trafficking process between two types of endothelial cells. Figure 6d panel plots the percentage with sub-categories providing more details in each category.

Heatmaps exhibiting gene expression profile show that there are more genes upregulated than downregulated in endocytosis, endosome–Golgi transport, exocytosis, SNARE, and other (Figures S15 and S16, Supporting Information). Endocytosis, endosome–Golgi transport (generally considered followed by nanoparticle exocytosis from the cell through secretory vesicles), and exocytosis are essential steps for nanoparticle transcytosis.[38] The trends observed in these categories are reverse with the expression pattern of the entire significantly changed gene population, in which more genes are downregulated than upregulated in HBTECs, suggesting the enrichment of upregulated genes in these processes.

The gene expression trend in the category endosome–lysosome transport is consistent with the whole cell expression pattern. The transport from endosome to lysosome is generally related to nanoparticle degradation and dysfunction due to the highly acidic environment and abundant hydrolytic enzymes, although some of the lysosomes can undergo exocytosis to release their undigested cargos as well.[38] In summary, the results of HBTECs and HMMECs with nanoparticle incubation suggest that tumor-associated endothelial cells are more active in transport and membrane trafficking processes. The sequencing results of HBTECs and HMMECs without nanoparticle incubation were also analyzed and the results exhibit similar trends as described above (Figures S18–S25, Supporting Information).

3. Conclusions

Our study revealed increased nanoparticle interactions and uptake by primary human tumor-associated endothelial cells compared to healthy tissue-derived endothelial cells for three different types of model nanoparticles with preclinical and clinical relevance. The internalization of gold nanoparticles occurred through active endocytosis, using all three major endocytic pathways: caveolin-mediated pathway, clathrin-mediated pathway, and macropinocytosis. The observed differential nanoparticle interaction efficiencies are likely attributed to intrinsic differences between the two types of endothelial cells. Specifically,

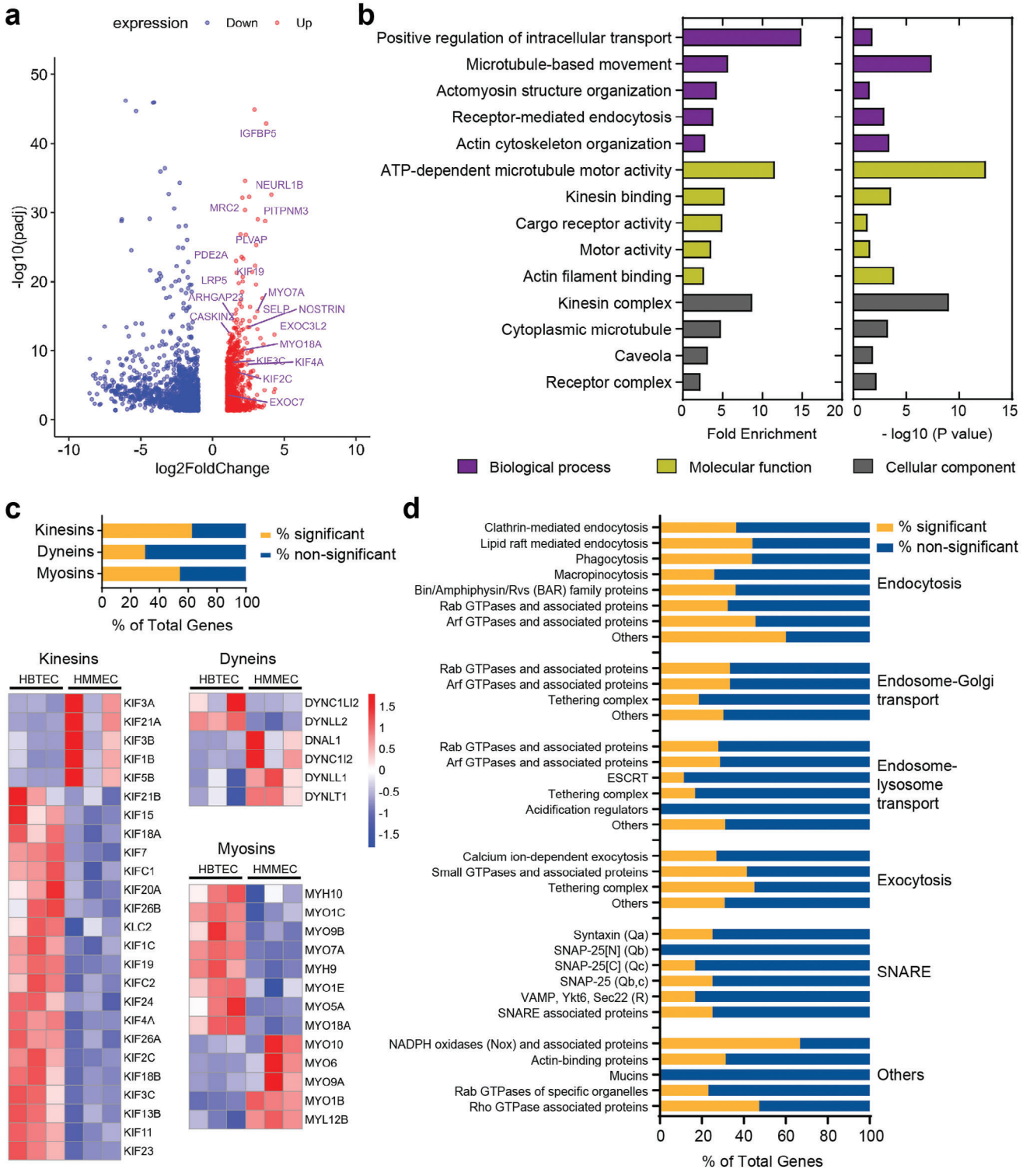

Figure 6. RNA-Seq analysis of tumor-associated and normal endothelial cells after 24-h incubation with gold nanoparticles. a) Volcano plot of the differentially expressed genes (DEGs) in HBTECs compared to HMMECs. Upregulated and downregulated genes are shown in red and blue dots. Some key genes related to nanoparticle transport are labeled. b) Gene ontology analysis of upregulated DEGs in HBTEC was performed using DAVID database. The enriched ontologies related to nanoparticle transport in biological process, molecular function, and cellular component were presented. c) Bar graph illustrating the percentage of statistically significant motor protein genes out of all sequenced motor protein genes. Heatmaps show the expression of statistically significant kinesins, dyneins, and myosins in HBTECs and HMMECs. The color scale is based on *z*-scores, where higher expression was colored in red while lower in blue. d) Bar graph illustrating the percentage of statistically different genes out of the sequenced genes within each category and subcategory of membrane trafficking. ESCRT, endosomal sorting complexes required for transport.

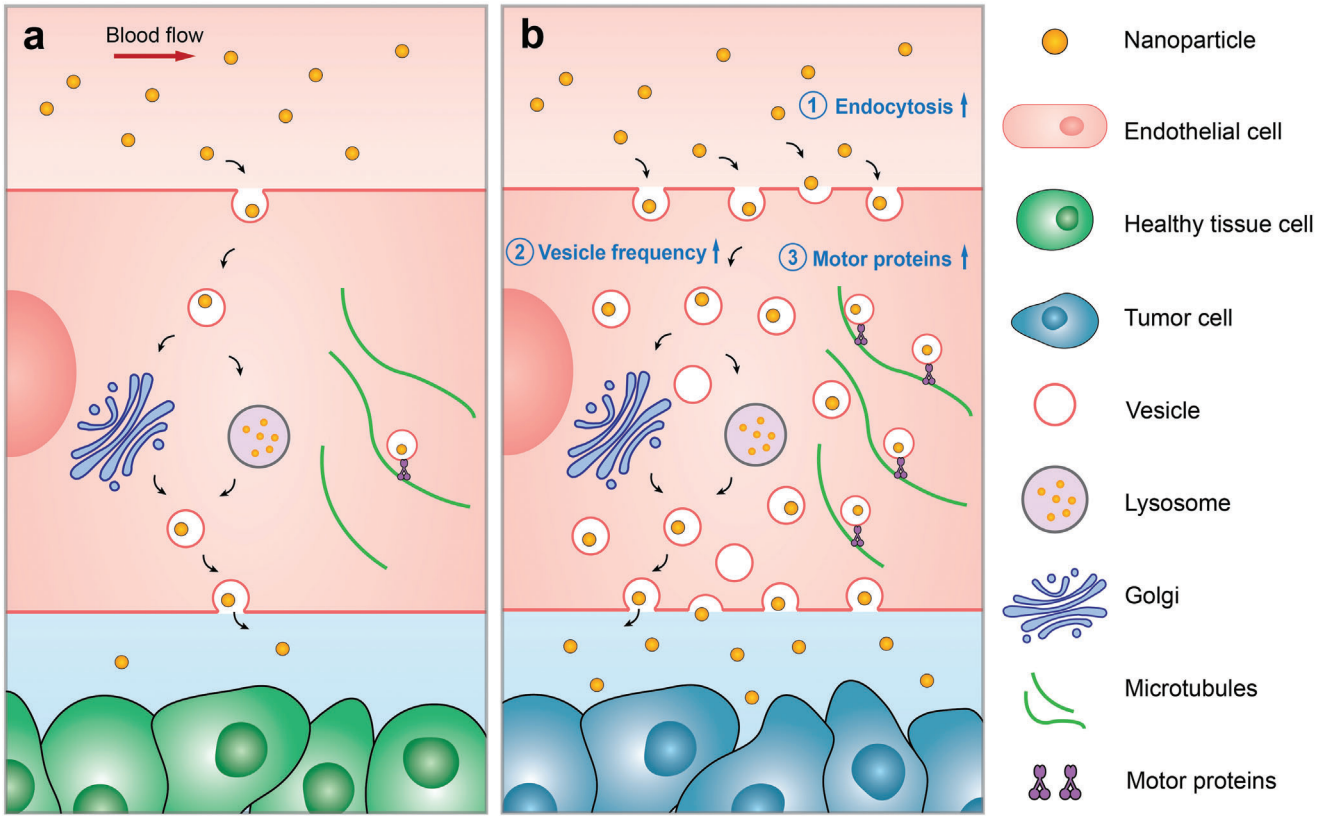

Scheme 1. a,b) Schematic illustration of a proposed nanoparticle transport processes in normal and tumor-associated endothelial cells. The tumor-associated endothelial cells generally exhibit higher endocytic activity, intracellular vesicle frequency, and enrichment of upregulated gene expression for motor proteins, endosome-Golgi transport, and exocytosis compared to normal endothelial cells. Further investigation into endocytosis, intracellular transport and exocytosis pathways of nanoparticles is necessary to fully support this proposed mechanism.

the tumor-associated endothelial cells demonstrated higher cellular transport activity than the healthy tissue-derived endothelial cells (**Scheme 1**). This proposed mechanism in Scheme 1 is supported by the observed increased endocytic pathway activity and intracellular vesicle frequency in tumor-associated endothelial cells. Furthermore, tumor-associated endothelial cells exhibited distinct gene expression patterns related to membrane trafficking processes, including endocytosis, motor protein-driven vesicle movement, endosome–Golgi transport, and exocytosis, further substantiating our proposed mechanism. Our findings establish the preferential interaction of tumor-associated endothelial cells with administered nanoparticles. A new class of safer, more effective, and more efficient next-generation cancer nanomedicines could exploit these preferential interactions for enhanced nanoparticle tumor delivery.

Our study suggests several important directions for future investigation. First, the process of nanoparticle transportation into solid tumors requires transcytosis, whereby nanoparticles traverse from the vessel lumen side to the tumor side of tumor-associated endothelial cells. However, our 2D in vitro culture system was unable to evaluate this transcytosis process. To address this limitation, future research should employ continuous endothelial cell monolayers cultured on transwell cell culture systems or other setups capable of quantifying transcytic nanoparticles. In addition, beyond endocytosis, a systematic comparison of intracellular transport and exocytosis pathways and efficiencies between tumor-associated and normal endothelial cells should be conducted. Second, the underlying factors contributing to the observed difference in transport activity between the two types of endothelial cells remain unclear but may be associated with the unique microenvironment in tumors. Future investigations could focus on identifying the specific factor(s) within the tumor microenvironment, such as growth factors (e.g., vascular endothelial growth factor) and cytokines, acidic pH, and hypoxia, which potentially influence nanoparticle transport in endothelial cells. Furthermore, in our work, the differences between the two types of primary endothelial cells persisted under the same in vitro cultural conditions, i.e., even after removal of the cells from their primary in vivo environment. The underlying reasons for this observation will require further investigation. Third, despite the use of human primary endothelial cells in our study, the cellular phenotype and behavior may still differ from the native in vivo conditions. Therefore, a thorough examination and comparison of transport features, including vesicle/vacuole structure and frequency, using primary human tissues will be necessary in future studies. Finally, the transport behavior of endothelial cells among different types of tumors should be evaluated due to the inherent heterogeneity of tumors and their microenvironments. A comprehensive understanding of the mechanisms behind nanoparticle transport by tumor-associated endothelial cells

and the specific factors enhancing this transport are fundamental and essential for advancing safer and more effective cancer nanomedicines.

Supporting Information

Supporting Information is available from the Wiley Online Library or from the author.

Acknowledgements

The authors acknowledge the assistance of Coline Furrer and Yuanhong Sun. In addition, the authors acknowledge the OU Mass Spectrometry, the Oklahoma Medical Research Foundation (OMRF) Imaging Core Facility, the OU Samuel Roberts Noble Microscopy Laboratory (SRML), and the Oklahoma COBRE in Cancer Imaging Research (Oklahoma Center of Medical Imaging for Translational Cancer Research). This work was supported in part by National Institutes of Health (NIH) MIRA R35 (1R35GM150758), NIH COBRE (P20GM135009), NIH (R01CA253391, NIH R01CA205348, NIH R01CA269897), National Science Foundation CAREER (2048130), OCAST HR20-106, HR16-0855, HF20-019, OVPRP Postdoc Match Program and Strategic Equipment Investment Program (SEIP).

Conflict of Interest

The authors declare no conflict of interest.

Data Availability Statement

The data that support the findings of this study are available in the supplementary material of this article.

Keywords

breast cancer, endocytosis, endothelial cells, nanomedicine, nanoparticle, solid tumors, transport

Received: March 18, 2024
Revised: April 19, 2024
Published online:

[1] L. Wang, S. Quine, A. N. Frickenstein, M. C. Lee, W. Yang, V. M. Sheth, M. D. Bourlon, Y. X. He, S. Lyu, L. Garcia-Contreras, Y. D. Zhao, S. Wilhelm, *Adv. Funct. Mater.* **2023**, *34*, 202308446.
[2] S. Wilhelm, A. J. Tavares, Q. Dai, S. Ohta, J. Audet, H. F. Dvorak, W. C. W. Chan, *Nat. Rev. Mater.* **2016**, *1*, 16014.
[3] a) Y. H. Cheng, C. L. He, J. E. Riviere, N. A. Monteiro-Riviere, Z. M. Lin, *ACS Nano* **2020**, *14*, 3075; b) F. Fan, B. Xie, L. H. Yang, *ACS Appl. Bio Mater.* **2021**, *4*, 7615.
[4] Q. Dai, S. Wilhelm, D. Ding, A. M. Syed, S. Sindhwani, Y. W. Zhang, Y. Y. Chen, P. MacMillan, W. C. W. Chan, *ACS Nano* **2018**, *12*, 8423.
[5] W. Poon, B. R. Kingston, B. Ouyang, W. Ngo, W. C. W. Chan, *Nat. Nanotechnol.* **2020**, *15*, 819.
[6] a) H. L. He, L. S. Liu, E. E. Morin, M. Liu, A. Schwendeman, *Acc. Chem. Res.* **2019**, *52*, 2445; b) L. Salvioni, M. A. Rizzuto, J. A. Bertolini, L. Pandolfi, M. Colombo, D. Prosperi, *Cancers* **2019**, *11*, 1855.
[7] a) T. J. Anchordoquy, Y. Barenholz, D. Boraschi, M. Chorny, P. Decuzzi, M. A. Dobrovolskaia, Z. S. Farhangrazi, D. Farrell, A. Gabizon, H. Ghandehari, B. Godin, N. M. La-Beck, J. Ljubimova, S. M. Moghimi, L. Pagliaro, J. H. Park, D. Peer, E. Ruoslahti, N. J. Serkova, D. Simberg, *ACS Nano* **2017**, *11*, 12; b) G. H. Petersen, S. K. Alzghari, W. Chee, S. S. Sankari, N. M. La-Beck, *J. Controlled Release* **2016**, *232*, 255.
[8] a) V. Sheth, L. Wang, R. Bhattacharya, P. Mukherjee, S. Wilhelm, *Adv. Funct. Mater.* **2021**, *31*, 2007363; b) S. M. Narum, T. Le, D. P. Le, J. C. Lee, N. D. Donahue, W. Yang, S. Wilhelm, in *Nanoparticles for Biomedical Applications* (Eds: E. J. Chung, L. Leon, C. Rinaldi), Elsevier, Amsterdam **2020**, Ch. 4, p. 37; c) Y. Y. Huai, M. N. Hossen, S. Wilhelm, R. Bhattacharya, P. Mukherjee, *Bioconjugate Chem.* **2019**, *30*, 2247.
[9] B. R. Kingston, Z. P. Lin, B. Ouyang, P. MacMillan, J. Ngai, A. M. Syed, S. Sindhwani, W. C. W. Chan, *ACS Nano* **2021**, *15*, 14080.
[10] A. C. Dudley, *Cold Spring Harbor Perspect. Med.* **2012**, *2*, a006536.
[11] J. Fang, W. Islam, H. Maeda, *Adv. Drug Delivery Rev.* **2020**, *157*, 142.
[12] S. Sindhwani, A. M. Syed, J. Ngai, B. R. Kingston, L. Maiorino, J. Rothschild, P. MacMillan, Y. W. Zhang, N. U. Rajesh, T. Hoang, J. L. Y. Wu, S. Wilhelm, A. Zilman, S. Gadde, A. Sulaiman, B. Ouyang, Z. Lin, L. S. Wang, M. Egeblad, W. C. W. Chan, *Nat. Mater.* **2020**, *19*, 566.
[13] a) L. Wang, S. Wilhelm, *Nat. Mater.* **2023**, *22*, 282; b) N. D. Donahue, H. Acar, S. Wilhelm, *Adv. Drug Delivery Rev.* **2019**, *143*, 68.
[14] X. H. Yao, Y. Zeng, *Front. Physiol.* **2023**, *14*, 1199225.
[15] R. Arvizo, R. Bhattacharya, P. Mukherjee, *Expert Opin. Drug Delivery* **2010**, *7*, 753.
[16] Y. Barenholz, *J. Controlled Release* **2012**, *160*, 117.
[17] M. D. Hu, X. Y. Li, Z. You, R. Cai, C. Y. Chen, *Adv. Mater.* **2023**, https://doi.org/10.1002/adma.202303266.
[18] A. N. Frickenstein, S. Mukherjee, T. Harcourt, Y. X. He, V. Sheth, L. Wang, Z. Malik, S. Wilhelm, *Anal. Bioanal. Chem.* **2023**, *415*, 4353.
[19] *NCCN Clinical Practice Guidelines in Oncology - Breast Cancer*. Version 5. **2023**.
[20] M. Verma, I. Ozer, W. Xie, R. Gallagher, A. Teixeira, M. Choy, *Nat. Rev. Drug Discovery* **2023**, *22*, 349.
[21] R. K. Thapa, J. O. Kim, *J. Pharm. Invest.* **2023**, *53*, 19.
[22] a) Y. Cao, Y. Gong, L. L. Liu, Y. W. Zhou, X. Fang, C. Zhang, Y. N. Li, J. Li, *J. Appl. Toxicol.* **2017**, *37*, 1359; b) M. I. Setyawati, C. Y. Tay, D. Docter, R. H. Stauber, D. T. Leong, *Chem. Soc. Rev.* **2015**, *44*, 8174.
[23] E. Betzig, J. K. Trautman, *Science* **1992**, *257*, 189.
[24] V. Sheth, X. X. Chen, E. M. Mettenbrink, W. Yang, M. A. Jones, O. M'Saad, A. G. Thomas, R. S. Newport, E. Francek, L. Wang, A. N. Frickenstein, N. D. Donahue, A. Holden, N. F. Mjema, D. E. Green, P. L. DeAngelis, J. Bewersdorf, S. Wilhelm, *ACS Nano* **2023**, *17*, 8376.
[25] a) F. Chen, P. W. Tillberg, E. S. Boyden, *Science* **2015**, *347*, 543; b) A. Klimas, B. R. Gallagher, P. Wijesekara, S. Fekir, E. F. DiBernardo, Z. Y. Cheng, D. B. Stolz, F. Cambi, S. C. Watkins, S. L. Brody, A. Horani, A. L. Barth, C. I. Moore, X. Ren, Y. X. Zhao, *Nat. Biotechnol.* **2023**, *41*, 858.
[26] F. B. Wang, B. L. Chen, B. Yan, Y. G. Yin, L. G. Hu, Y. Liang, M. Y. Song, G. B. Jiang, *J. Am. Chem. Soc.* **2019**, *141*, 14043.
[27] a) A. Aliyandi, S. Satchell, R. E. Unger, B. Bartosch, R. Parent, I. S. Zuhorn, A. Salvati, *Int. J. Pharm.* **2020**, *587*, 119699; b) J. Blechinger, A. T. Bauer, A. A. Torrano, C. Gorzelanny, C. Bräuchle, S. W. Schneider, *Small* **2013**, *9*, 3970.
[28] a) M. C. Gerbod-Giannone, L. Dallet, G. Naudin, A. Sahin, M. Decossas, S. Poussard, O. Lambert, *Biochim. Biophys. Acta, Gen. Subj.* **2019**, *1863*, 830; b) A. Krishna, D. Sengupta, *Biophys. J.* **2019**, *116*, 69.
[29] a) Z. M. Chen, S. L. Schmid, *J. Cell Biol.* **2020**, *219*, e202005126; b) T. Kirchhausen, D. Owen, S. C. Harrison, *Cold Spring Harbor Perspect. Biol.* **2014**, *6*, a016725; c) S. J. Royle, *Cell. Mol. Life Sci.* **2006**, *63*, 1823.
[30] I. Taskaeva, N. Bgatova, *Microvasc. Res.* **2021**, *133*, 104094.

[31] a) S. Kumari, M. G. Swetha, S. Mayor, *Cell Res.* **2010**, *20*, 256; b) X. P. Lin, Z. Z. Xiao, T. Chen, S. H. Liang, H. Q. Guo, *Front. Oncol.* **2020**, *10*, 317; c) X. Q. Liu, D. Ghosh, *Int. J. Nanomed.* **2019**, *14*, 6589.
[32] a) V. Ganapathy, M. Thangaraju, P. D. Prasad, *Pharmacol. Ther.* **2009**, *121*, 29; b) D. Feng, J. A. Nagy, A. M. Dvorak, H. F. Dvorak, *Microvasc. Res.* **2000**, *59*, 24.
[33] D. E. Tylawsky, H. Kiguchi, J. Vaynshteyn, J. Gerwin, J. K. Shah, T. Islam, J. A. Boyer, D. R. Boué, M. Snuderl, M. B. Greenblatt, Y. Shamay, G. P. Raju, D. A. Heller, *Nat. Mater.* **2023**, *22*, 391.
[34] N. Hirokawa, Y. Noda, Y. Tanaka, S. Niwa, *Nat. Rev. Mol. Cell Biol.* **2009**, *10*, 682.
[35] M. A. Titus, *Cold Spring Harbor Perspect. Biol.* **2018**, *10*, a021972.
[36] H. L. Sweeney, E. L. F. Holzbaur, *Cold Spring Harbor Perspect. Biol.* **2018**, *10*, a021931.
[37] C. Ghilardi, G. Chiorino, R. Dossi, Z. Nagy, R. Giavazzi, M. Bani, *BMC Genomics* **2008**, *9*, 201.
[38] a) J. Liu, Y. Y. Liu, C. S. Li, A. E. Cao, H. F. Wang, *Nanomaterials* **2023**, *13*, 2215; b) R. Sakhtianchi, R. F. Minchin, K. B. Lee, A. M. Alkilany, V. Serpooshan, M. Mahmoudi, *Adv. Colloid Interface Sci.* **2013**, *201*, 18.